JACS
JOURNAL OF THE AMERICAN CHEMICAL SOCIETY
pubs.acs.org/JACS
Communication

A Distinct Spin Structure and Giant Baromagnetic Effect in MnNiGe Compounds with Fe-Doping

Feiran Shen,[#] Houbo Zhou,[#] Fengxia Hu,[*] Jian-Tao Wang,[*] Hui Wu, Qingzhen Huang, Jiazheng Hao, Zibing Yu, Yihong Gao, Yuan Lin, Yangxin Wang, Cheng Zhang, Zhuo Yin, Jing Wang,[*] Sihao Deng, Jie Chen, Lunhua He,[*] Tianjiao Liang, Ji-Rong Sun, Tongyun Zhao, and Baogen Shen[*]

Cite This: *J. Am. Chem. Soc.* 2021, 143, 6798−6804

ABSTRACT: Spin structure of a magnetic system results from the competition of various exchange couplings. Pressure-driven spin structure evolution, through altering interatomic distance, and hence, electronic structure produces baromagnetic effect (BME), which has potential applications in sensor/actuator field. Here, we report a new spin structure(CyS-AFM^b) with antiferromagnetic(AFM) nature in Fe-doped $Mn_{0.87}Fe_{0.13}NiGe$. Neutron powder diffraction (NPD) under in situ hydrostatic pressure and magnetic field was conducted to reveal the spin configuration and its instabilities. We discovered that a pressure higher than 4 kbar can induce abnormal change of Mn(Fe)−Mn(Fe) distances and transform the CyS-AFM^b into a conical spiral ferromagnetic(FM) configuration(45°-CoS-FM^a) with easily magnetized but shortened magnetic moment by as much as 22%. The observed BME far exceeds previous reports. Our first-principles calculations provide theoretical supports for the enhanced BME. The compressed lattice by pressure favors the 45°-CoS-FM^a and significantly broadened 3d bandwidth of Mn(Fe) atoms, which leads to the shortened magnetic moment and evolution of spin structure.

External pressure is a direct means to affect material lattice. Altering interatomic distance and, hence, electronic structure by pressure can produce abundant physical properties, such as baromagnetic effect (BME), barocaloric effect,[1−4] transition among metal, semiconductor and insulator,[5−7] enhanced ferroelectricity[8] and self-trapped exciton emission,[9] and even room-temperature superconductivity.[10] Among them, BME, that is, pressure-induced change of magnetic moment, has potential applications in the fields of intelligent instruments, sensors, actuators, and magnetoelectric (ME) devices utilizing interfacial strain.[11] The materials with strong cross-correlations between volume and spin order provide excellent platform for exploring BME. In antiperovskite $Mn_3Ga_{0.95}N_{0.94}$ with 3D geometric frustration in the spin configuration, pressure driven spin reorientation from antiferromagnetic-(AFM) Γ^{5g} to ferrimagnetic(FIM) M-1 leads to a large BME.[12] The equivalent maximal baromagnetic coefficient (BMC, $d = |dM/dP|_H$)[13] is $d \sim 1.92$ emu·g^{-1}·kbar^{-1} under a 1−5 T magnetic field (see unit conversion in Supporting Information SI-1). This is the largest observed up to date by utilizing spin structure evolution. Exploring amplified BMC and extending the BME to a low magnetic field region is of significance from viewpoint of practical applications.

Mn-based ternary metallic alloys MnMX (M = transition element, X = main element) have recently gained much attention owing to rich physical effects.[14−16] Topologically protected vortex-like spin structure, that is, magnetic biskyrmions, was demonstrated in an off-stoichiometric alloy $(Mn_{0.5}Ni_{0.5})_{65}Ga_{35}$,[17−19] which poses canted ferromagnetic-(FM) ground state and persists Ni_2In-type hexagonal structure in entire temperature range. On the other hand, some MnMX alloys lose the structural stability and undergo a martensitic structural transition from hexagonal Ni_2In-type austenite(space group $P6_3/mmc$) to TiNiSi-type orthorhombic martensite-(space group $Pnma$). The martensite shows a variety of spin structure,[20−24] critically depending on the Mn−Mn bond lengths, particularly on the Mn−Mn(d_1) with direct exchange[20,21] (Figure 1a), which provides excellent platform for exploring pressure regulated spin-structure and hence giant BME.

The stoichiometric MnNiGe undergoes a martensitic transition around $T_S \sim 420$ K, and the martensite displays spiral AFM structure.[24] However, the AFM coupling is so robust that the change of Mn−Mn distance by a pressure as high as 8kbar is unable to alter the AFM state.[25] So, no BME occurs in MnNiGe. Fortunately, the substitution of Mn with Fe introduces FM coupling.[26] We found that the spin-structure of a Fe-doped $Mn_{0.87}Fe_{0.13}NiGe$ becomes susceptible to Mn(Fe)−Mn(Fe) distance. A new cycloidal spiral AFM structure (denoted as CyS-AFM^b thereafter), different from the AFM configuration of the undoped MnNiGe, was found. Neutron powder diffraction (NPD) studies under variable hydrostatic pressure, magnetic field, and temperature (SI-2) revealed the characteristics and instabilities of the CyS-AFM^b. Rietveld refinements indicate Fe atoms randomly occupy Mn

Received: March 11, 2021
Published: May 3, 2021

https://doi.org/10.1021/jacs.1c02694
J. Am. Chem. Soc. 2021, 143, 6798−6804

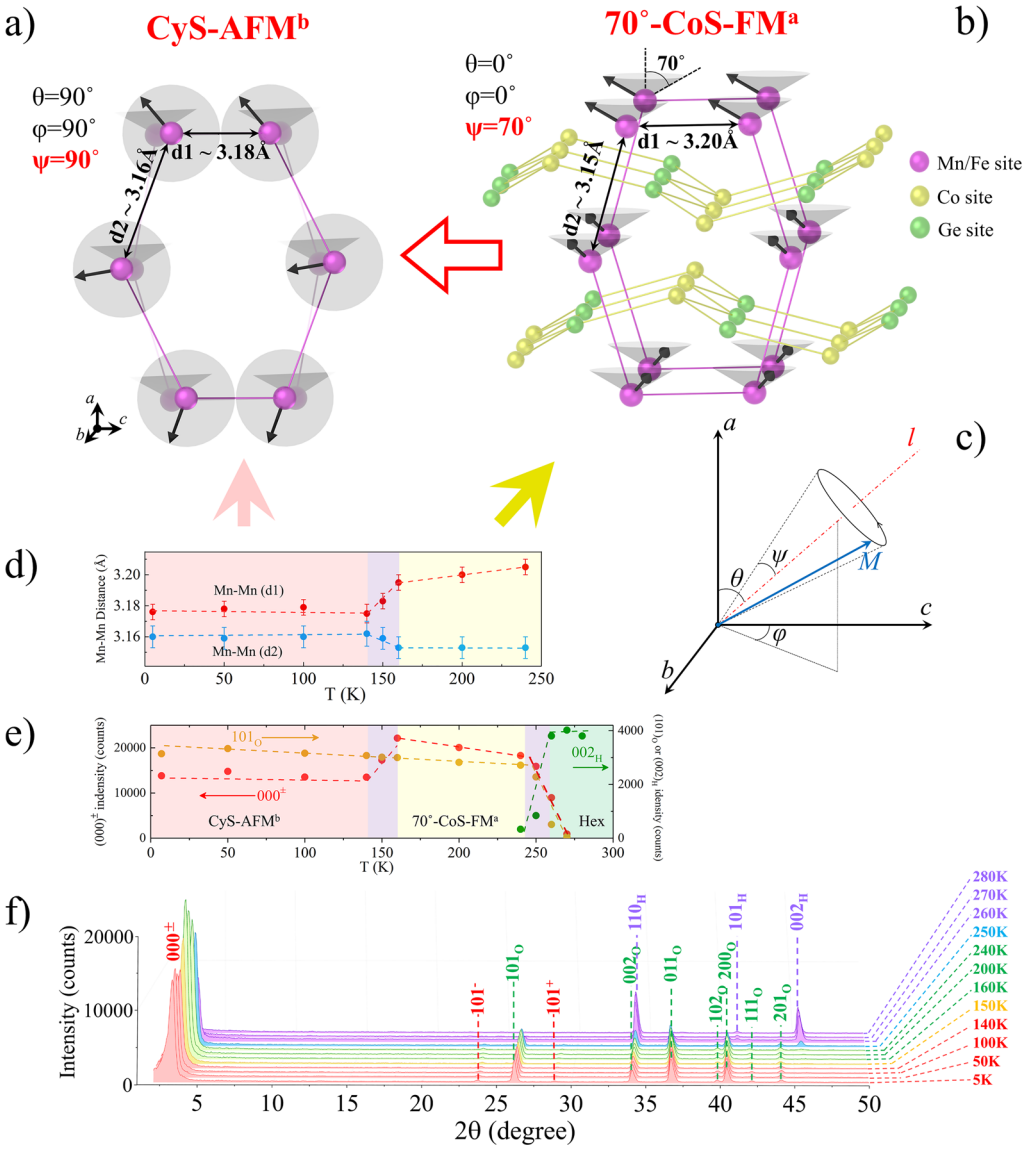

Figure 1. Sketch of (a) the conversion from 70°-CoS-FM[a] to CyS-AFM[b], (b) the 70°-CoS-FM[a], and (c) the spherical coordinate. Variation of (d) Mn−Mn distances and (e) the peak intensity of $(000)^{\pm}$ magnetic satellite (red), orthorhombic (101) crystal reflection (yellow), and hexagonal (002) crystal reflection (green) with temperature. (f)Temperature-dependent NPD patterns.

sites and the ratio Fe ~ 12.5(3)% approaches to the nominal compositions (SI-3). A pressure higher than 4 kbar can transform it into a conical spiral FM (45°-CoS-FM[a]) with easily magnetized but shortened magnetic moment. Giant BME was observed under either low magnetic field (≤0.35 T) or 2−5 T. First-principles calculations (SI-4) provide further theoretical supports for the enhanced BME.

To precisely describe the configuration of spin-structure, spherical coordinate (SI-5) is used, as shown in Figure 1c. NPD refinements indicate that, in the 150−250 K zone, the $Mn_{0.87}Fe_{0.13}NiGe$ possesses an incommensurate conical spiral FM structure with $\psi = 70°$, $\theta = 0°$, and $\varphi = 0°$ (denoted as 70°-CoS-FM[a], Figure 1b), in line with the previously reported.[27] Surprisingly, a new spiral spin-structure (Figure 1a) is developed below ~50K, which was not observed before in the Fe-doped MnNiGe. The optimal parameters are $\psi = 90°$, $\theta = 90°$, and $\varphi = 90°$, that is, the cone axis $\boldsymbol{l}$ is along the b axis, and the magnetic moment is perpendicular to the $\boldsymbol{l}$, corresponding to a cycloidal spiral structure. While the magnetic moment is confined on Mn(Fe) sites with $\mu_{(Mn/Fe)} = 3.06(2)\ \mu_B$ at 5 K, and the propagation vector $k = [0.16731(5), 0, 0]$ along the a_{orth} axis.

Such a spiral structure shows AFM nature (namely, CyS-AFM[b]) but differs from the AFM configuration of the stoichiometric MnNiGe (SI-6). The formation of the new CyS-AFM[b] is closely related to the step change of Mn−Mn(d_1) and Mn−Mn(d_2) distances around the spin structure transition point T_m ~ 150 K (Figure 1d, a), although no anomaly occurs in the lattice parameters there (see Figure S1c and discussion in SI-7). The step increase of magnetic satellite peak $(000)^{\pm}$ around T_m ~ 150 K(read from NPD patterns Figure 1f) is also indicative of spin structural transition (red line in Figure 1e and SI-2)

Unlike the robust AFM coupling in MnNiGe,[24,25] the formed CyS-AFM[b] in $Mn_{0.87}Fe_{0.13}NiGe$ behaves susceptible against either magnetic field (H) or pressure (P). Macroscopic magnetic measurements (M−H curves) at 5 K (Figure 2a) indicate that a low critical magnetic field H_C ~ 0.35 T can

https://doi.org/10.1021/jacs.1c02694
J. Am. Chem. Soc. 2021, 143, 6798−6804

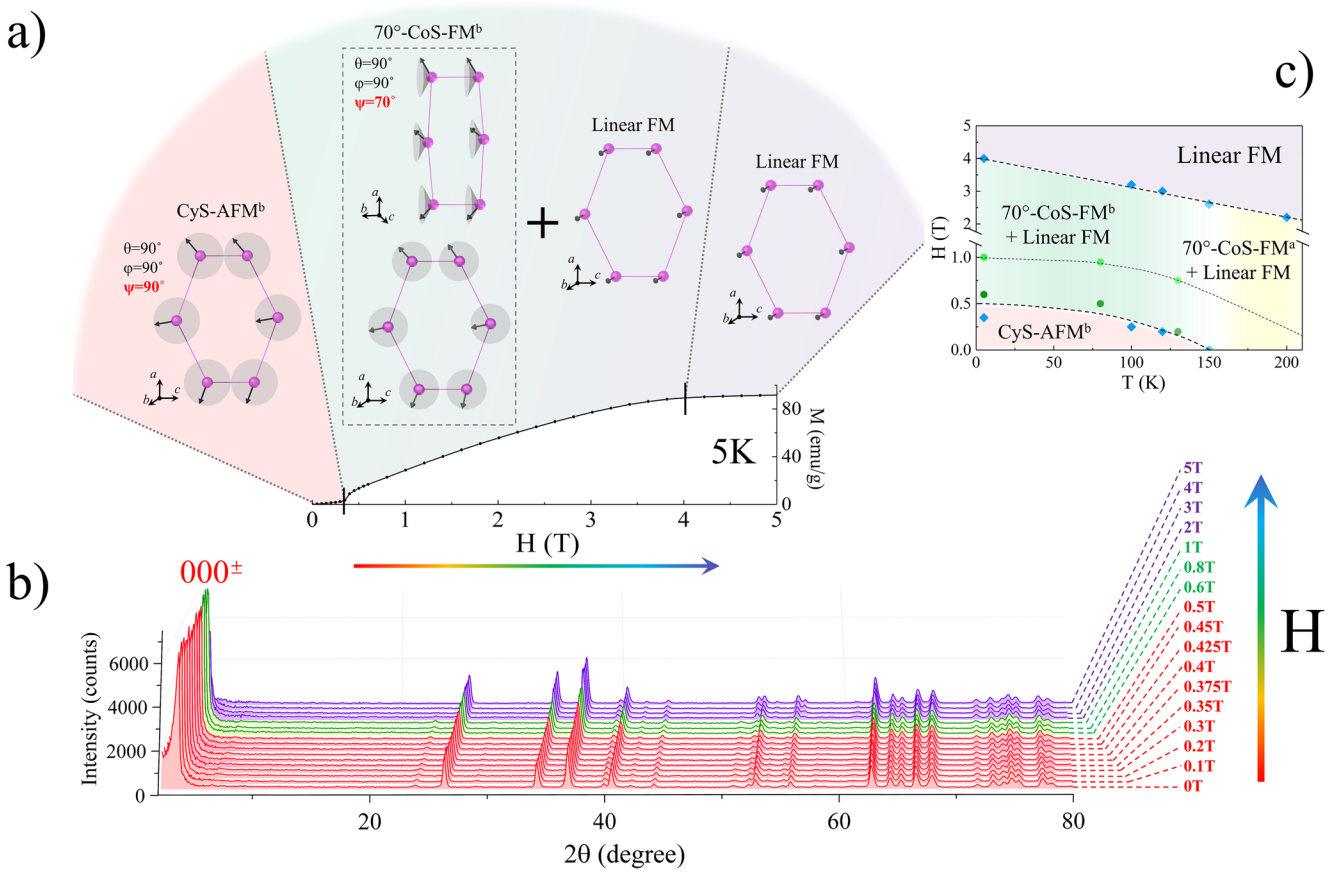

Figure 2. (a) $M-H$ curve at 5 K with the sketch of spin structure evolution with H. (b) Variable magnetic field NPD patterns at 5 K and (c) phase diagram (SI-8).

induce a metamagnetic transition with a step rise of magnetization (M). M then increases almost linearly until saturation with saturated moment $M_s \sim 3.05\ \mu_B$, unlike the spontaneous magnetizing behavior of a typical FM magnet. To reveal the evolution process of spin-structure, NPD measurements under variable magnetic fields were performed at 5 K (Figure 2b). Careful refinements indicate that the CyS-AFM^b evolves into the conical spiral FM 70°-CoS-FM^b with $\psi = 70°$, $\theta = 90°$, $\varphi = 90°$ at around ~0.6 T,and then to a linear FM structure aligning b axis (see Figure 2a, c and details in SI-8).

More intriguingly, the new CyS-AFM^b in $Mn_{0.87}Fe_{0.13}NiGe$ is no longer insensitive to stress. Figure 3a display the $M-H$ curves measured under variable pressures at different temperatures. At the CyS-AFM^b region ($T \leq 150$ K), $P \sim 1.8$kbar pressure cannot remarkably alter the magnetizing process. The shape of M-H curves persists almost the same while the saturated moment remains unchanged, except a slight reduction of saturated magnetic field (H_s). Meanwhile, the critical field Hc triggering the transition from CyS-AFM^b to 70°-CoS-FM^b also keeps unchanged at the same temperature. One exception is the situation of 150 K, where the 1.8 kbar pressure can revive the CyS-AFM^b with a small $H_c \sim 0.1$ T (see inset of Figure 3a(4)), though increasing temperature up to 150 K have already collapsed the CyS-AFM^b with $H_c = 0$. It means pressure stabilizes the new CyS-AFM^b.

Further increasing pressure up to 6.0kbar makes the magnetizing process completely different from the situation at atmospheric pressure (Figure 3a(1−4)). The isothermal $M-H$ curves at $T \leq 150$ K become easily magnetized particularly at low field region $H \leq 0.5$ T, similar to the spontaneous magnetizing behavior of a typical FM magnet, while the saturated moment notably reduces by as much as 22% at 5 K (Table S3). Continuously increasing pressure to 8.3 kbar leads to further easier magnetized and further reduction of saturated moment, while the shape of $M-H$ curves does not change too much (Figure 3a(1−4)). The distinct magnetizing behavior at $P = 0$ and $P \geq 6$kbar leads to the occurrence of large BME, $\Delta M_{HP} = M(P,H)_T - M(0,H)_T$, not only at the magnetic field higher than H_s but also in the low field region, while the sign of BME changes, as shown in Figure 3a(6−10).

At low magnetic field (H), positive BME appears below 150 K, which peaks exactly around the H_c. Typically, the BME under a low $H = 0.35$ T reaches +32.0 and +40.5emu/g, while the corresponding BMC $d = |\Delta M_{HP}/\Delta P|_{H,T} \sim 5.34$ and ~4.88emu·g^{-1}·kbar^{-1}, under 6.0 kbar and 8.3 kbar, respectively. With increasing H, the sign of BME turns to be negative, and the BME reaches the negative maximum at around the H_s and then keeps almost unchanged with further increasing H (Figure 3a(6−10)). The negative BME at 150 and 200 K reaches its maximum at $H_s \sim 2.6$ and 2.2 T, while the magnitude under 6.0 and 8.3 kbar is −30.1 and −35.5 emu/g (150 K) and −54.2 and −62.7 emu/g (200 K) and corresponding BMC $d \sim 5.02$ and 4.27 emu·g^{-1}·kbar^{-1} (150 K) and 9.03 and 7.55 emu·g^{-1}·kbar^{-1} (200 K), respectively (see details in SI-9).

Obviously, the BME in $Mn_{0.87}Fe_{0.13}NiGe$ is more attractive compared to the $Mn_3Ga_{0.95}N_{0.94}$ previously reported.[12] The maximal BMC $d = 9.03$ emu·g^{-1}·kbar^{-1} at 2.2 T is 4.7 times

https://doi.org/10.1021/jacs.1c02694
J. Am. Chem. Soc. 2021, 143, 6798−6804

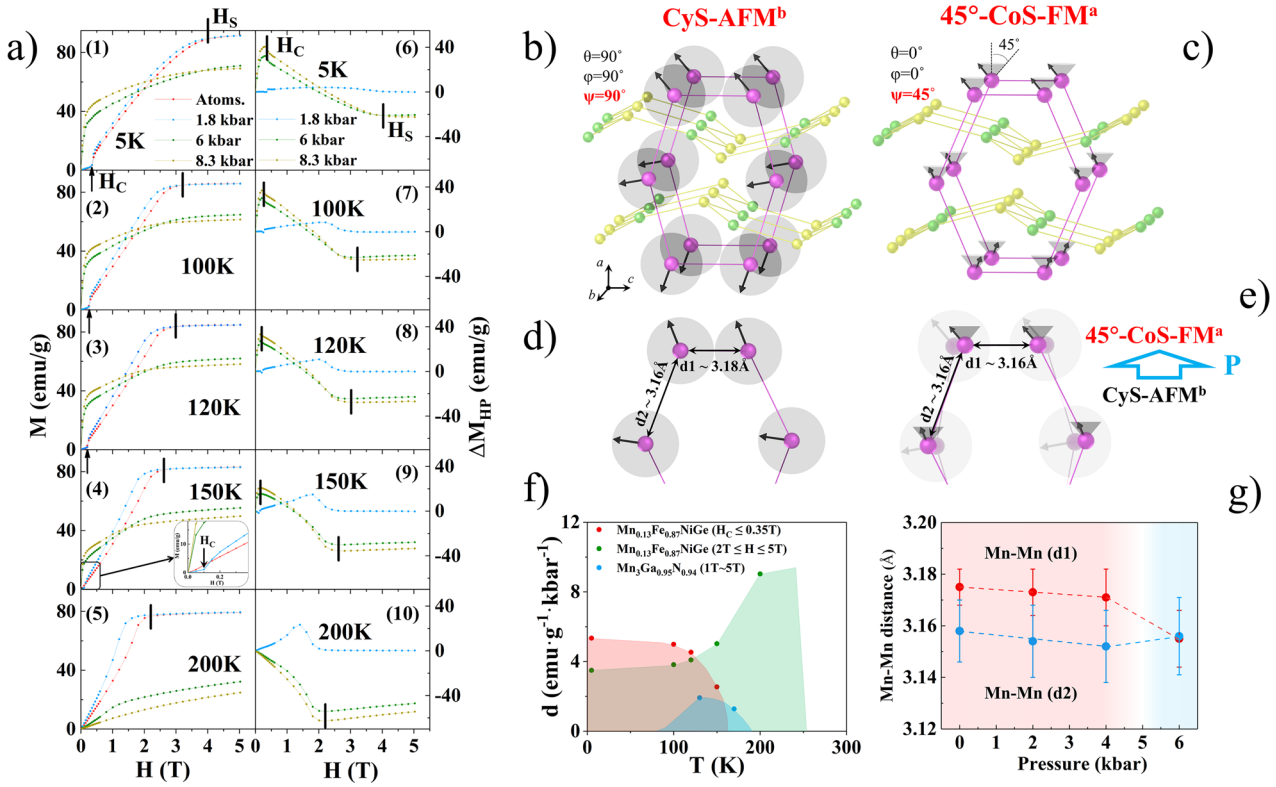

Figure 3. (a) $M-H$ curves and the BME (ΔM_{HP}) under selected hydrostatic pressures at 5, 100, 120, 150, and 200 K, respectively. The sketch of (b, d) the CyS-AFM[b] and (c, e) the 45°-CoS-FM[a]. (f) BMC d of $Mn_{0.87}Fe_{0.13}NiGe$ under $H_c \leq 0.35$ T (red) and 2 T $\leq H \leq$ 5 T (green), compared with that of $Mn_3Ga_{0.95}N_{0.94}$ [12, SI-1] under 1−5 T (blue). (g) Variation of Mn−Mn distances with pressure at 120 K.

Table 1. Refined Magnetic Structure with Spherical Angles, $M_{Mn(Fe)}$, Mn−Mn distances (d_1, d_2), and Martensite Fraction (Wt(Ort)) from NPD at 120 K under Different Pressures[a]

	pressure	0 kbar	2 kbar	4 kbar	6 kbar
NPD	spin structure	CyS-AFM[b]	CyS-AFM[b]	CyS-AFM[b]	45°-CoS-FM[a]
	θ	90°	90°	90°	0°
	φ	90°	90°	90°	0°
	ψ	90°	90°	90°	45°
	$M_{Mn(Fe)}$ (μ_B)	2.80(3)	2.78(3)	2.79(3)	2.08(3)
	d_1 (Å)	3.175(7)	3.173(9)	3.171(11)	3.155(11)
	d_2 (Å)	3.158(12)	3.154(14)	3.152(14)	3.156(15)
	Wt_{Ort} (%)	99(1)	99(1)	98(1)	98(1)
	Rwp	5.70	6.67	7.12	7.15
	χ^2	3.86	1.66	2.02	2.11
M−H	pressure	0 kbar	1.8 kbar	-	6 kbar
	M_S (μ_B)	2.83	2.83	-	2.07

[a] M_s from $M-H$ curves at 120 K is listed for comparison.

greater than that of $Mn_3Ga_{0.95}N_{0.94}$, while the temperature range (0−250 K) is also significantly wider (Figure 3f). For $Mn_3Ga_{0.95}N_{0.94}$, the maximal ΔM_{HP} is ∼+14.4 emu/g at 130 K/7.5 kbar, equivalent BMC d ∼1.92 emu·g^{-1}·kbar^{-1} within temperature window ∼115 K (75−190 K) (see SI-1).[12]

To reveal the mechanism of large BME in $Mn_{0.87}Fe_{0.13}NiGe$, NPD under variable hydrostatic pressure was performed at 120 K in CyS-AFM[b] region. Careful refinements indicated the spiral configuration, as well as the spin moment, remains almost unchanged under $P \leq$ 4kbar (Table 1). However, as the pressure reaches 6.0 kbar, the optimal parameters tunes to be ψ = 45°, θ = 0°, and φ = 0°, corresponding to a conical spiral structure, we name it 45°-CoS-FM[a] (Figure 3c) (see details in SI-10). Meanwhile, the refined moment drops from 2.80(3) μ_B (0 kbar) to 2.08(3) μ_B (6.0 kbar). All these are in line with the macroscopic magnetic measurements (Figure 3a), noting that the refined moments ($M_{Mn(Fe)}$) from NPD are nearly the same as the saturation moments (M_s) from the $M-H$ curves at corresponding conditions (Tables 1 and S3). Such good consistency also illustrates the reliability of refined results. The pressure driven transition from CyS-AFM[b] (Figure 3b) to 45°-CoS-FM[a] (Figure 3c) is closely related to the altered local atomic environments by pressure (Figure 3d, e and detailed discussion in SI-7). NPD refinements indeed detected abnormal changes of Mn−Mn (d_1) and Mn−Mn (d_2) distances between 4 and 6 kbar (Figure 3g), although no obvious anomaly can be identified in the lattice parameters (Figure S9). The Mn−Mn (d_1) and Mn−Mn (d_2) distances

https://doi.org/10.1021/jacs.1c02694
J. Am. Chem. Soc. 2021, 143, 6798−6804

remain monotonously compressed at $P \leq 4.0$ kbar but show abrupt change with pressure further increasing to 6.0 kbar.

To theoretically explain the pressure driven instability of spin structure, total energy was calculated by first-principles calculations with PW91 generalized gradient approximation[28,29] for CyS-AFM^b and the derived 45°-CoS-FM^a by pressure (see Computational Details in SI-4). The atomic positions refined from NPD data at 120 K/6.0 kbar were input, and the cycloidal/conical spiral model was constructed with the unit cell periods obtained from NPD data. Figure 4a shows

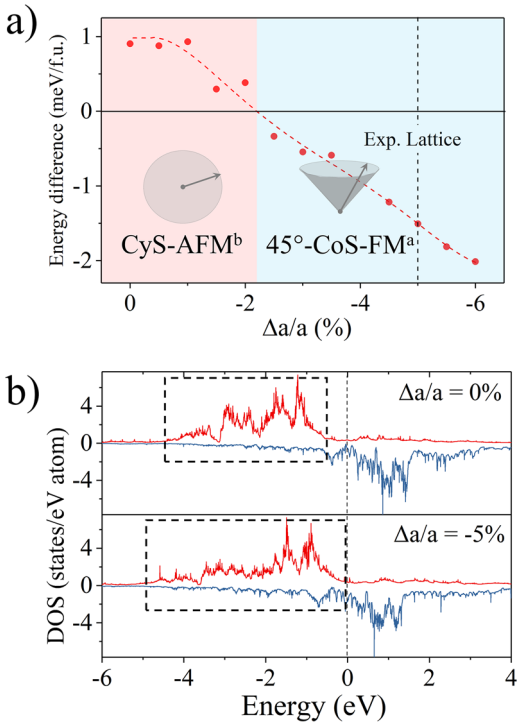

Figure 4. (a) Difference between the total energies of CyS-AFM^b and 45°-CoS-FM^a. (b) Partial electronic density of states of high spin state at $\Delta a/a = 0\%$ and low spin state at $\Delta a/a = -5\%$.

the energy difference per formula unit($\Delta E = E_{45°\text{-CoS-FM}^a} - E_{\text{CyS-AFM}^b}$) against lattice strain $\Delta a/a$ between 0 and −6%. The results demonstrate that the 45°-CoS-FM^a with compressed lattice is more stable than the CyS-AFM^b, noting an energy gain of 1.5 meV/f.u. at the experimental lattice parameters. Moreover, for the shortened magnetic moment by pressure, we calculated the partial electronic density of states(DOS) of high spin state at $\Delta a/a = 0\%$ and low spin state at $\Delta a/a = -5\%$, where Mn(Fe) magnetic moment at 5 K was adopted, that is, $M_{\text{Mn(Fe)}} \sim 3.06\ \mu_B$ (0 kbar) and $M_{\text{Mn(Fe)}} \sim 2.37\ \mu_B$ (6.0 kbar) based on NPD and macroscopic magnetic measurements (Table S3). The result is shown in Figure 4b. For the high spin state at $\Delta a/a = 0\%$, the up-spin state is basically full and roughly distributed in the range of −4.4 to −0.5 eV. While, for the low spin state at $\Delta a/a = -5\%$, the bandwidth of Mn 3d bands is strongly broadened, and the up-spin state distributed in the range of −4.8 to 0 eV (Figure 4b). The significantly broadened 3d bandwidth should be responsible for the notably shortened magnetic moment. With the lattice compressed, the overlap of Mn 3d orbitals will be stronger that makes the 3d orbitals of Mn atoms more itinerant. As a result, the d−d hybrid bands become broader, and the exchange splitting of the Mn 3d states become weaker, hence leading to reduction of magnetic moments.[20,30,31]

To conclude, a new spiral spin structure(CyS-AFM^b) with AFM nature was found in Fe-doped $Mn_{0.87}Fe_{0.13}NiGe$ alloys. NPD under in situ pressure and magnetic field reveal the spin configuration and its instability. A low magnetic field 0.35 T can make the CyS-AFM^b transform to a conical spiral FM with angle 70° (70°-CoS-FM^b), accompanied by a step rise of magnetization. More importantly, the new CyS-AFM^b is no longer insensitive to stress compared to the MnNiGe without Fe-doping. A pressure higher than 4 kbar induces abnormal change of Mn(Fe)−Mn(Fe) distances hence transform the CyS-AFM^b into a conical spiral ferromagnetic configuration (45°-CoS-FM^a) with easily magnetized but much shortened magnetic moment. As a result, giant BME was observed under either a low magnetic field or a field of 2−5 T. The maximal BMC appears to be ~5.34 emu·g^{-1}·kbar^{-1} under 0.35 T while ~9.03 emu·g^{-1}·kbar^{-1} under 2.2 T in a wide temperature range, which all far exceed those of the previous reported $Mn_3Ga_{0.95}N_{0.94}$.[12] First-principles calculations provide theoretical supports for the spin structure transition and the shortened magnetic moment by pressure. This work would provide insightful directions for exploring novel BME materials.

■ ASSOCIATED CONTENT

Supporting Information

The Supporting Information is available free of charge at https://pubs.acs.org/doi/10.1021/jacs.1c02694.

Experimental details, computational methods, and more NPD details under variable magnetic fields and pressure (PDF)

■ AUTHOR INFORMATION

Corresponding Authors

Fengxia Hu − *Institute of Physics, Chinese Academy of Sciences, Beijing 100190, China; School of Physical Sciences, University of Chinese Academy of Sciences, Beijing 101408, China; Songshan Lake Materials Laboratory, Dongguan, Guangdong 523808, China;* orcid.org/0000-0003-0383-0213; Email: fxhu@iphy.ac.cn

Jian-Tao Wang − *Institute of Physics, Chinese Academy of Sciences, Beijing 100190, China; School of Physical Sciences, University of Chinese Academy of Sciences, Beijing 101408, China; Songshan Lake Materials Laboratory, Dongguan, Guangdong 523808, China*; Email: wjt@iphy.ac.cn

Jing Wang − *Institute of Physics, Chinese Academy of Sciences, Beijing 100190, China; School of Physical Sciences, University of Chinese Academy of Sciences, Beijing 101408, China; Fujian Innovation Academy, Chinese Academy of Sciences, Fuzhou, Fujian 350108, China;* orcid.org/0000-0001-5458-6711; Email: wangjing@iphy.ac.cn

Lunhua He − *Institute of Physics, Chinese Academy of Sciences, Beijing 100190, China; Songshan Lake Materials Laboratory, Dongguan, Guangdong 523808, China; Spallation Neutron Source Science Center, Dongguan 523803, China*; Email: lhhe@iphy.ac.cn

Baogen Shen − *Institute of Physics, Chinese Academy of Sciences, Beijing 100190, China; School of Physical Sciences, University of Chinese Academy of Sciences, Beijing 101408, China; Songshan Lake Materials Laboratory, Dongguan, Guangdong 523808, China; Ganjiang Innovation Academy,*

https://doi.org/10.1021/jacs.1c02694
J. Am. Chem. Soc. 2021, 143, 6798−6804

Chinese Academy of Sciences, Ganzhou, Jiangxi 341000, China; Email: shenbg@iphy.ac.cn

Authors

Feiran Shen − *Institute of Physics, Chinese Academy of Sciences, Beijing 100190, China; School of Physical Sciences, University of Chinese Academy of Sciences, Beijing 101408, China*

Houbo Zhou − *Institute of Physics, Chinese Academy of Sciences, Beijing 100190, China; School of Physical Sciences, University of Chinese Academy of Sciences, Beijing 101408, China*

Hui Wu − *NIST Center for Neutron Research, National Institute of Standards and Technology, Gaithersburg, Maryland 20899, United States;* orcid.org/0000-0003-0296-5204

Qingzhen Huang − *NIST Center for Neutron Research, National Institute of Standards and Technology, Gaithersburg, Maryland 20899, United States*

Jiazheng Hao − *Institute of Physics, Chinese Academy of Sciences, Beijing 100190, China; Spallation Neutron Source Science Center, Dongguan 523803, China*

Zibing Yu − *Institute of Physics, Chinese Academy of Sciences, Beijing 100190, China; School of Physical Sciences, University of Chinese Academy of Sciences, Beijing 101408, China*

Yihong Gao − *Institute of Physics, Chinese Academy of Sciences, Beijing 100190, China; School of Physical Sciences, University of Chinese Academy of Sciences, Beijing 101408, China*

Yuan Lin − *Institute of Physics, Chinese Academy of Sciences, Beijing 100190, China; School of Physical Sciences, University of Chinese Academy of Sciences, Beijing 101408, China*

Yangxin Wang − *Institute of Physics, Chinese Academy of Sciences, Beijing 100190, China; Spallation Neutron Source Science Center, Dongguan 523803, China*

Cheng Zhang − *Institute of Physics, Chinese Academy of Sciences, Beijing 100190, China; School of Physical Sciences, University of Chinese Academy of Sciences, Beijing 101408, China*

Zhuo Yin − *Institute of Physics, Chinese Academy of Sciences, Beijing 100190, China; School of Physical Sciences, University of Chinese Academy of Sciences, Beijing 101408, China*

Sihao Deng − *Spallation Neutron Source Science Center, Dongguan 523803, China*

Jie Chen − *Spallation Neutron Source Science Center, Dongguan 523803, China*

Tianjiao Liang − *Spallation Neutron Source Science Center, Dongguan 523803, China*

Ji-Rong Sun − *Institute of Physics, Chinese Academy of Sciences, Beijing 100190, China; School of Physical Sciences, University of Chinese Academy of Sciences, Beijing 101408, China; Songshan Lake Materials Laboratory, Dongguan, Guangdong 523808, China*

Tongyun Zhao − *Institute of Physics, Chinese Academy of Sciences, Beijing 100190, China; Ganjiang Innovation Academy, Chinese Academy of Sciences, Ganzhou, Jiangxi 341000, China*

Complete contact information is available at: https://pubs.acs.org/10.1021/jacs.1c02694

Author Contributions

#F.S. and H.Z. contributed equally.

Notes

The authors declare no competing financial interest.

■ ACKNOWLEDGMENTS

This research was partially supported by the BT-1 neutron powder diffractometer at NIST Center for Neutron Research. This work was supported by the Science Center of the National Science Foundation of China (52088101), National Key Research and Development Program of China (2019YFA0704900, 2020YFA0711502, 2017YFB0701903, 2018YFA0305704, 2017YFB0702702, 2017YFA0303601, 2017YFA0206300), the National Natural Sciences Foundation of China (U1832219, 51771223, 51971240, 11934016, 11921004), the Strategic Priority Research Program (B), and key program of the Chinese Academy of Sciences (CAS).

■ REFERENCES

(1) Mañosa, L.; González-Alonso, D.; Planes, A.; Bonnot, E.; Barrio, M.; Tamarit, J. L.; Aksoy, S.; Acet, M. Giant solid-state barocaloric effect in the Ni-Mn-In magnetic shape-memory alloy. *Nat. Mater.* **2010**, *9*, 478−481.

(2) Mañosa, L.; González-Alonso, D.; Planes, A.; Barrio, M.; Tamarit, J. L.; Titov, I. S.; Acet, M.; Bhattacharyya, A.; Majumdar, S. Inverse barocaloric effect in the giant magnetocaloric La-Fe-Si-Co compound. *Nat. Commun.* **2011**, *2*, 595.

(3) Matsunami, D.; Fujita, A.; Takenaka, K.; Kano, M. Giant barocaloric efect enhanced by the frustration of the antiferromagnetic phase in Mn_3GaN. *Nat. Mater.* **2015**, *14*, 73−78.

(4) Li, B.; Kawakita, Y.; Ohira-Kawamura, S.; Sugahara, T.; Wang, H.; Wang, J.; Chen, Y.; Kawaguchi, S. I.; Kawaguchi, S.; Ohara, K.; Li, K.; Yu, D.; Mole, R.; Hattori, T.; Kikuchi, T.; Yano, S.-i.; Zhang, Z.; Zhang, Z.; Ren, W.; Lin, S.; Sakata, O.; Nakajima, K.; Zhang, Z. Colossal barocaloric effects in plastic crystals. *Nature* **2019**, *567*, 506−510.

(5) Imada, M.; Fujimori, A.; Tokura, Y. Metal-insulator transitions. *Rev. Mod. Phys.* **1998**, *70*, 1039−1263.

(6) Matsuoka, T.; Shimizu, K. Direct observation of a pressure-induced metal-to-semiconductor transition in lithium. *Nature* **2009**, *458*, 186−189.

(7) Nayak, A. P.; Bhattacharyya, S.; Zhu, J.; Liu, J.; Wu, X.; Pandey, T.; Jin, C. Q.; Singh, A. K.; Akinwande, D.; Lin, J. F. Pressure-induced semiconducting to metallic transition in multilayered molybdenum disulphide. *Nat. Commun.* **2014**, *5*, 3731.

(8) Wang, J.; Wylie-Van Eerd, B.; Sluka, T.; Sandu, C.; Cantoni, M.; Wei, X. K.; Kvasov, A.; McGilly, L. J.; Gemeiner, P.; Dkhil, B.; Tagantsev, A.; Trodahl, J.; Setter, N. Negative-pressure-induced enhancement in a freestanding ferroelectric. *Nat. Mater.* **2015**, *14*, 985.

(9) Li, Q.; Chen, Z. W.; Yang, B.; Tan, L.; Xu, B.; Han, J.; Zhao, Y. S.; Tang, J.; Quan, Z. W. Pressure-induced remarkable enhancement of self-trapped exciton emission in one-dimensional $CsCu_2I_3$ with tetrahedral units. *J. Am. Chem. Soc.* **2020**, *142*, 1786−1791.

(10) Snider, E.; Dasenbrock-Gammon, N.; McBride, R.; Debessai, M.; Vindana, H.; Vencatasamy, K.; Lawler, K. V.; Salamat, A.; Dias, R. P. Room-temperature superconductivity in a carbonaceous sulfur hydride. *Nature* **2020**, *586*, 373−377.

(11) Lukashev, P.; Sabirianov, R. F.; Belashchenko, K. Theory of the piezomagnetic effect in Mn-based antiperovskites. *Phys. Rev. B: Condens. Matter Mater. Phys.* **2008**, *78*, 184414.

(12) Shi, K.; Sun, Y.; Yan, J.; Deng, S.; Wang, L.; Wu, H.; Hu, P.; Lu, H.; Malik, M. I.; Huang, Q.; Wang, C. Baromagnetic Effect in antiperovskite $Mn_3Ga_{0.95}N_{0.94}$ by neutron powder diffraction analysis. *Adv. Mater.* **2016**, *28*, 3761−3767.

(13) Kekalo, I. B.; Nemova, O. Y.; Taranitchev, V. E. Piezomagnetic coefficients of amorphous alloys with low magnetostriction. *J. Magn. Magn. Mater.* **1996**, *157*, 181−182.
(14) Zhao, Y.-Y.; Hu, F.-X.; Bao, L.-F.; Wang, J.; Wu, H.; Huang, Q.-Z.; Wu, R.-R.; Liu, Y.; Shen, F.-R.; Kuang, H.; Zhang, M.; Zuo, W.-L.; Zheng, X.-Q.; Sun, J.-R.; Shen, B.-G. Giant negative thermal expansion in bonded MnCoGe-based compounds with Ni_2In-type hexagonal structure. *J. Am. Chem. Soc.* **2015**, *137*, 1746−1749.
(15) Wu, R.-R.; Bao, L.-F.; Hu, F.-X.; Wu, H.; Huang, Q.-Z.; Wang, J.; Dong, X.-L.; Li, G.-N.; Sun, J.-R.; Shen, F.-R.; Zhao, T.-Y.; Zheng, X.-Q.; Wang, L.-C.; Liu, Y.; Zuo, W.-L.; Zhao, Y.-Y.; Zhang, M.; Wang, X.-C.; Jin, C.-Q.; Rao, G.-H.; Han, X.-F.; Shen, B.-G. Giant barocaloric effect in hexagonal Ni_2In-type Mn-Co-Ge-In compounds around room temperature. *Sci. Rep.* **2015**, *5*, 18027.
(16) Trung, N. T.; Zhang, L.; Caron, L.; Buschow, K. H. J.; Bruck, E. Giant magnetocaloric effects by tailoring the phase transitions. *Appl. Phys. Lett.* **2010**, *96*, 172504.
(17) Wang, W. H.; Zhang, Y.; Xu, G. Z.; Peng, L. C.; Ding, B.; Wang, Y.; Hou, Z. P.; Zhang, X. M.; Li, X. Y.; Liu, E. K.; Wang, S. G.; Cai, J. W.; Wang, F. W.; Li, J. Q.; Hu, F. X.; Wu, G. H.; Shen, B. G.; Zhang, X. X. A centrosymmetric hexagonal magnet with superstable biskyrmion magnetic nanodomains in a wide temperature range of 100−340 K. *Adv. Mater.* **2016**, *28*, 6887−6893.
(18) Loudon, J. C.; Twitchett-Harrison, A. C.; Cortés-Ortuño, D.; Birch, M. T.; Turnbull, L. A.; Stefancic, A.; Ogrin, F. Y.; Burgos-Parra, E. O.; Bukin, N.; Laurenson, A.; Popescu, H.; Beg, M.; Hovorka, O.; Fangohr, H.; Midgley, P. A.; Balakrishnan, G.; Hatton, P. D. Do images of biskyrmions show type-II bubbles? *Adv. Mater.* **2019**, *31*, 1806598.
(19) Li, X.; Zhang, S.; Li, H.; Venero, D. A.; White, J. S; Cubitt, R.; Huang, Q.; Chen, J.; He, L.; van der Laan, G.; Wang, W.; Hesjedal, T.; Wang, F. Oriented 3D magnetic biskyrmions in MnNiGa bulk crystals. *Adv. Mater.* **2019**, *31*, 1900264.
(20) Gercsi, Z.; Sandeman, K. G. Structurally driven metamagnetism in MnP and related Pnma compounds. *Phys. Rev. B: Condens. Matter Mater. Phys.* **2010**, *81*, 224426.
(21) Gercsi, Z.; Hono, K.; Sandeman, K. G. Designed metamagnetism in $CoMnGe_{1-x}P_x$. *Phys. Rev. B: Condens. Matter Mater. Phys.* **2011**, *83*, 174403.
(22) Bazela, W.; Szytula, A.; Todorovic, J.; Zieba, A. Crystal and magnetic structure of the $NiMnGe_{1-n}Si_n$ system. *Phys. Status Solidi A* **1981**, *64*, 367−378.
(23) Szytuła, A.; Pędziwiatr, A.T.; Tomkowicz, Z.; Bażela, W. Crystal and magnetic structure of CoMnGe, CoFeGe, FeMnGe and NiFeGe. *J. Magn. Magn. Mater.* **1981**, *25*, 176−186.
(24) Bazela, W.; Szytula, A.; Todorovic, J.; Tomkowicz, Z.; Zieba, A. Crystal and magnetic structure of NiMnGe. *Phys. Status Solidi A* **1976**, *38*, 721.
(25) Anzai, S.; Ozawa, K. Coupled nature of magnetic and structural transition in MnNice under pressure. *Phys. Rev. B: Condens. Matter Mater. Phys.* **1978**, *18*, 2173.
(26) Liu, E.; Wang, W.; Feng, L.; Zhu, W.; Li, G.; Chen, J.; Zhang, H.; Wu, G.; Jiang, C.; Xu, H.; de Boer, F. Stable magnetostructural coupling with tunable magnetoresponsive effects in hexagonal ferromagnets. *Nat. Commun.* **2012**, *3*, 873.
(27) Shen, F. R.; Zhou, H. B.; Hu, F. X.; Wang, J. T.; Deng, S. H.; Wang, B. T.; Wu, H.; Huang, Q. H.; Wang, J.; Chen, J.; He, L. H.; Hao, J. Z.; Yu, Z. B.; Liang, F. X.; Liang, T. J.; Sun, J. R.; Shen, B. G. Cone-spiral magnetic ordering dominated lattice distortion and giant negative thermal expansion in Fe-doped MnNiGe compounds. *Mater. Horiz.* **2020**, *7*, 804−810.
(28) Deng, S. H.; Sun, Y.; Wang, L.; Shi, Z. X.; Wu, H.; Huang, Q. Z.; Yan, J.; Shi, K. W.; Hu, P. W.; Zaoui, A.; Wang, C. Frustrated triangular magnetic structures of Mn_3ZnN: Applications in thermal expansion. *J. Phys. Chem. C* **2015**, *119*, 24983−24990.
(29) Perdew, J. P.; Wang, Y. Accurate and simple analytic representation of the electron-gas correlation energy. *Phys. Rev. B: Condens. Matter Mater. Phys.* **1992**, *45*, 13244−13249.
(30) Wang, J. T.; Li, Z. Q.; Zhou, L.; Kawazoe, Y.; Wang, D. S. Stabilities of spin configuration and exchange interactions in (Cr, Mn, Fe)/Ag monatomic multilayers. *Phys. Rev. B: Condens. Matter Mater. Phys.* **1999**, *59*, 6974−6978.
(31) Wang, J. T.; Li, Z. Q.; Sun, Q.; Kawazoe, Y. First-principles study of the magnetic and the electronic properties of Fe_m/Au_n multilayers. *J. Magn. Magn. Mater.* **1998**, *183*, 42−48.

https://doi.org/10.1021/jacs.1c02694
J. Am. Chem. Soc. 2021, 143, 6798−6804